

Overview of Recent Progress and Future in GAMMA 10/PDX Project

Y. Nakashima^{1, a)}, T. Imai¹⁾, M. Sakamoto¹⁾, I. Katanuma¹⁾, T. Kariya¹⁾,
M. Yoshikawa¹⁾, N. Ezumi¹⁾, R. Minami¹⁾, M. Hirata¹⁾, J. Kohagura¹⁾,
T. Numakura¹⁾, R. Ikezoe¹⁾, K. Ichimura¹⁾, X. Wang¹⁾, M. Ichimura¹⁾
and GAMMA 10/PDX group¹⁾

¹⁾Plasma Research Center, University of Tsukuba, Tsukuba, Ibaraki 305-8577, Japan

^{a)}Corresponding author: nakashma@prc.tsukuba.ac.jp

Abstract. This paper presents an overview of the recent progress of GAMMA 10/PDX project. In the GAMMA 10/PDX project, development of fusion reactor relevant research related to magnetic mirror devices has been conducted. One of the main objectives is divertor simulation studies under the similar condition of actual fusion devices, which contributes to comprehensive development strategy towards the divertor plasma physics and plasma wall interaction (PWI) studies. The recent progress of this research is that an additional plasma heating (ICRF and ECH) significantly increased the ion flux up to $3.3 \times 10^{23} / \text{m}^2 \text{s}$ at the end-mirror exit, which proved an effectiveness of additional plasma heating for generating high ion flux from the mirror end. Superimposing a short pulse of ECH produces the maximum heat flux of 21 MW/m^2 by improving the west plug ECH antenna system, which exceeds the heat-load of ITER divertor plates. In detached plasma formation experiments using the divertor simulation experimental module (D-module), comparison of various radiator gases (Xe, Ar, Ne, N₂) injected into D-module showed that Xe was the most effective gas on electron cooling and reduction of heat and ion fluxes. In the development of high-power gyrotrons, a number of electron cyclotron heating experiments using high-power gyrotrons have been performed under strong collaboration and we made a remarkable contribution to LHD and QUEST. A MW-level dual frequency gyrotron is also successfully being developed and 13.8 MW at 28GHz and 0.87 MW at 35 GHz is achieved. Multi-channel/multi-pass Thomson scattering system has been developed and simultaneous measurement of radially 6 points with 10 Hz can be available. The multi-pass function of this system also improved the measurement accuracy and time resolution. Microwave interferometer system has been developed in the GAMMA 10/PDX end-cell, which contributes to detailed diagnostics for divertor simulation plasmas in D-module.

1. INTRODUCTION

In the development of nuclear fusion research, importance of studies on boundary plasma and plasma-wall interactions is increasingly recognized. The boundary plasma exists in the complex system under the influence of various atomic and molecular processes in the intermediate region between the hot core plasma and the low temperature divertor plate exposed to high heat flux. Furthermore, the Scrape Off Layer (SOL) plasma in toroidal devices has an open magnetic field configuration and shows the distinctive characteristics in contrast to the core plasma. In such circumstances, it is considered that the boundary plasma studies using linear devices with the similar in magnetic field configuration to SOL plasmas contributes to the understanding of divertor physics and plasma-wall interaction studies in toroidal devices.

In the Plasma Research Center, University of Tsukuba, extensive efforts aiming magnetic nuclear fusion has been made by using a tandem mirror device. Figure 1 shows the schematic view of the GAMMA 10 tandem mirror device. GAMMA 10 is the world largest axi-symmetrized tandem mirror device with a total length of 27 m [1]. GAMMA 10 consists of a central-cell with a simple mirror configuration, minimum-B anchor-cells with baseball coils and plug/barrier-cells in which the axial plasma confining potentials are formed. An initial seed-plasma injected from both end-cells is built-up by using ICRF waves irradiated from the antennae in the central-cell and hot plasmas with the density of 10^{18} m^{-3} are produced. A strong ion heating with ICRH using

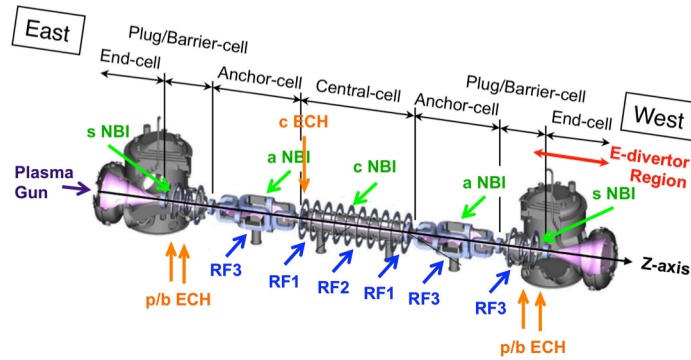


FIGURE 1. Schematic view of the GAMMA 10 tandem mirror device and E-divertor region.

another antenna perpendicularly heat the ions up to several keV. For this target plasma, EC wave produced by four gyrotrons installed in both east and west plug/barrier-cells, respectively is applied and the plasma confinement is improved by the potential formation axially and radially. In GAMMA 10, high-power plasma heating devices are equipped and a new experimental activity has been started for studies on boundary plasma and divertor simulation. In this activity, making best use of the above resources together with the modification of GAMMA 10, the GAMMA 10/PDX project has been started, where PDX denotes Potential control and Divertor simulation eXperiment [2].

One of the most important research subjects in GAMMA 10/PDX project is the divertor simulation by using high heat-flux and particle flux plasma flowing out of the end-mirror coil. This divertor plasma simulator is called E-Divertor and various experimental activities have been extensively performed since 2008 [3-8]. So far, in the E-divertor research, we have investigated characteristics of high heat and particle fluxes produced at the end-mirror exit and both the ion temperature of 100~400 eV and the particle flux of 10^{22} particles/s·m² were achieved by using ICRF wave [6]. Superimposing ECH into the plasma significantly increased the heat flux, which attained the peak heat-flux more than 10 MW/m² on axis during ECH of 380 kW [7].

In Fig. 2, operation parameter ranges of linear divertor simulators are plotted as a space of ion energy vs ion flux together with areas of the first wall, SOL plasmas and that of divertor [9]. The observed ion energy range in E-divertor is comparable to that of the SOL parameters, which cannot be attained for other divertor simulators. We contribute to achieving the steady-state operation of detached plasma in ITER/Demo reactors by obtaining knowledge for the generation and stable control of detached plasma and investigating the mechanism of radiation cooling and impurity transport due to the radiator gas injection. Recently by the massive injection of hydrogen and noble gases, we have succeeded in achieving detached plasma formation in E-divertor region [10, 11].

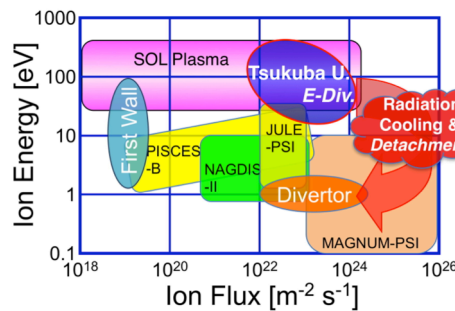


FIGURE 2. Ion energy vs ion flux in various linear devices in the world [9], together with that of E-divertor.

Development of high-power gyrotrons, which is another important subject in GAMMA 10/PDX project, has progressed under the joint program with NIFS (National Institute of Fusion Science) in collaboration with QST (National Institute for Quantum and Radiological Science and Technology) and TETD (Toshiba Electron Tube & Device Co.). ECH by using gyrotron is an essential method for potential confinement and for obtaining high electron temperature in tandem mirror devices [12, 13]. A gyrotron is also a powerful tool for ECH and ECCD. In the plasma research center, development of gyrotron with a frequency of 28 GHz has been started. Two 0.2 MW and three 0.5 MW gyrotrons have been installed in GAMMA 10. In 2009, development of a 28 GHz 1 MW gyrotron was started for GAMMA 10/PDX, achieving an output power of 1.05 MW [14, 15]. Output powers of

1.25 MW was achieved with this 28GHz 1 MW gyrotron after modification of the magnetic injection gun (MIG) in 2012 and improvement of the power supply attained 1.38 MW in 2015.

Thomson scattering (TS) diagnostic is a powerful method for measuring electron temperature and density plasmas and has been applied to low-density plasmas in the GAMMA 10/PDX edge region [16, 17]. In order to improve the low signal to noise ratio, multi-pass TS has been proposed and continuous efforts for upgrading system have been continued. An application of electron density measurement in E-divertor region using a multi-channel microwave interferometer system contribute to the clarification of the plasma characteristics in the E-divertor region and characterization of wave structure in the central-cell, respectively.

In this paper, recent results of GAMMA 10/PDX project are described in section 2-4. In section 5, the summary and future prospects are presented.

2. DIVERTOR SIMULATION RESEARCH

2.1. High Heat and Particle Flux Generation Experiments

Characteristics of end-loss particles produced plasmas from the central-cell have been investigated in early stage of E-divertor studies. A set of combined detector system consists of a calorimeter and a directional Langmuir probe has been installed at 30 cm downstream from the end-mirror coil and simultaneous measurement of particle flux and heat flux has been carried out. The diamagnetism measured in the central-cell increases with the ICRF power for ion heating in the mid-plane (RF2) and resultant ion temperature along the magnetic field line increase linearly. In the case of particle flux, a linear relationship between ion flux measured with ELIEA and the central-cell line density has been clarified [5]. Recently additional plasma heating experiment using a new ICRF system in the anchor-cell (RF3) was carried out in order to improve the performance of E-divertor.

Figure 3(a) shows the schematic view of additional heating experiments aiming the enhancement of particle flux of end-loss plasma flow by using ICRF and ECH. In this experiment, the plasma is built up by the RF1 wave and the additional heating pulse is firstly applied with RF2 wave using antennae installed at both anchor-cells together with RF3 at the plug/barrier-cell. In Fig. 3(b), the time behavior of plasma electron line-density measured at the central-cell and anchor-cells (upper figure) is shown together with that of ion flux measured with ELIEA at both east and west ends (lower figure). Note that the ion flux is converted to the particle flux at the position of the Langmuir probe (30 cm downstream of the end-mirror coil). As shown in the figure, it is observed that line-densities in both the anchor-cells and the central-cell increase by 3 times and 2.5 times, respectively due to the application of RF3 at both anchor-cells and the resultant ion flux at the west end is attained to be $1.7 \times 10^{23} / \text{m}^2 \text{s}$. Furthermore, the ion flux at the west end is significantly enhanced by applying the east plug/barrier ECH without increasing the central-cell plasma density and attained the maximum particle flux of $3.3 \times 10^{23} / \text{m}^2 \text{s}$.

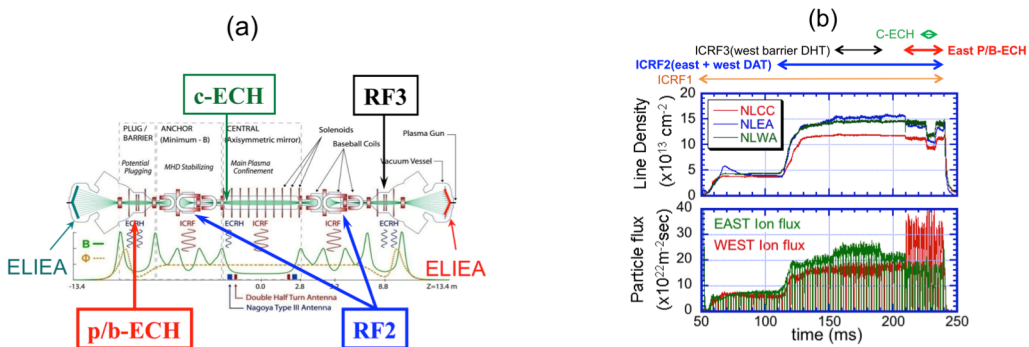


FIGURE 3. (a) Schematic view of additional heating experiments using ICRF wave and ECH, (b) Time behavior of the plasma electron line-density measured at the central-cell and the anchor-cells (upper figure), the ion flux measured with ELIEA on both ends (lower figure). The ion flux is converted to the particle flux at the position of the Langmuir probe (30 cm downstream of the end-mirror coil).

In Fig. 4, ion flux data measured with the west ELIEA are plotted against the central-cell line density, NLCC. From the figure, it is noted that the ion flux is almost increases with NLCC under the various additional heating scenarios using central and anchor RF's, central NBI and central ECH. The important point is that abrupt increase of ion flux is recognized due to the east plug/barrier ECH without any increase of the plasma density in

the central-cell and anchor-cells. This result indicates that the potential enhancement due to the east plug/barrier ECH may reflect the end-loss ions of the east side toward the west end-cell and/or increases the end-loss particles toward the loss cone in the velocity space of mirror trapped ions in the central-cell. From the measured data of east ELIEA signal, the end-loss plugging with the east plug/barrier ECH is not sufficiently observed and it is considered that the potential effect together with the ionization due to the application of plug /barrier ECH can contribute to the enhancement of ion flux. Further investigations of end-loss plasma flow and much more analyses are needed for understanding these phenomena.

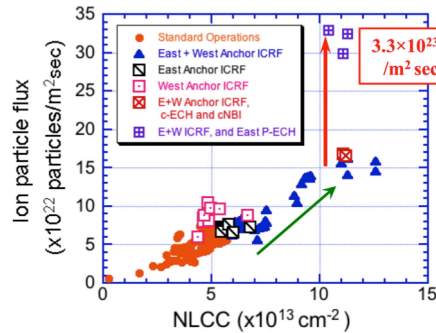


FIGURE 4. Dependence of ion flux measured with the west ELIEA on the central cell line-density under various heating conditions. The value of the ion flux is the same as in Fig.3(b).

High heat flux generation experiments using ECH have been performed in the early state of the project. The plug ECH was used to generate the high-energy electron-flow to the end-mirror exit. The heat flux measured with the calorimeter installed at 30 cm downstream from the end-mirror exit showed the high intensity almost comparable to a 0.2 sec. ICRF plasma discharges in spite of the short pulse (~10 ms) injection of ECH. In Fig. 5, the evaluated heat flux during ECH is plotted as a function of the plug ECH power. As increasing the ECH power, almost linear increase was observed in each experimental period. Last year a short pulse injection of ECH achieved the highest heat flux about 17 MW/m², which exceeds the heat-load level of ITER divertor plates in steady state. In this spring, by installation of a newly improved antenna in west plug ECH system, the maximum heat flux of 21 MW/m² has been achieved. It is expected that installation of both plug ECH antennae together with MW power gyrotrons under development will attain the heat flux of more than 30 MW/m² in near future.

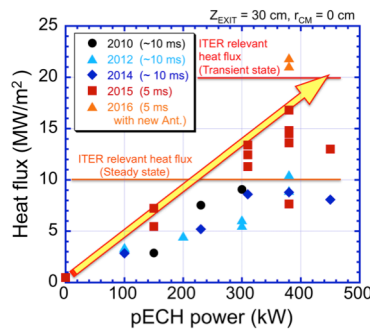


FIGURE 5. Dependence of heat flux measured with the calorimeter near the west end-mirror exit (30 cm downstream) on the applied ECH power.

2.2. Characterization of Detached Plasma Using Various Radiator Gases

In 2012, a dedicated instrument for divertor simulation studies was installed in E-divertor region [7]. Figure 6 shows the schematic view of the device in the GAMMA 10 west end-cell. This device is called D-module and consists of rectangular box made of stainless steel. In D-module, two tungsten plates (350×300 mm) are mounted in V-shaped with their variable open-angle from 15 to 80 degree. D-module is equipped with gas injection system for investigating radiation cooling mechanism toward the plasma detachment in D-module. In order to evaluate the electron density, temperature and the heat flux on to the target plate, arrays of Langmuir probes and calorimeters are installed on the each upper and lower tungsten plates, respectively. A pair of calorimeter and Langmuir probe (corner detectors) is also located behind a small gap of the V-shaped corner for

investigating the radiation cooling mechanism and plasma detachment. For the measurement of neutral pressure of introduced neutral gas pressure into D-module, an ASDEX-type ionization gauge was recently installed on the D-module. ASDEX gauge is a fast ionization gauge capable of operation in the strong magnetic field and in the pressure range expected in plasma detachment, 0.1 ~ 10 Pa [16]. The gauge has been calibrated by using hydrogen and argon gases in a test chamber and the sensitivity of the gauge in the magnetic field was also evaluated under the magnetic field of the GAMMA 10/PDX end-cell.

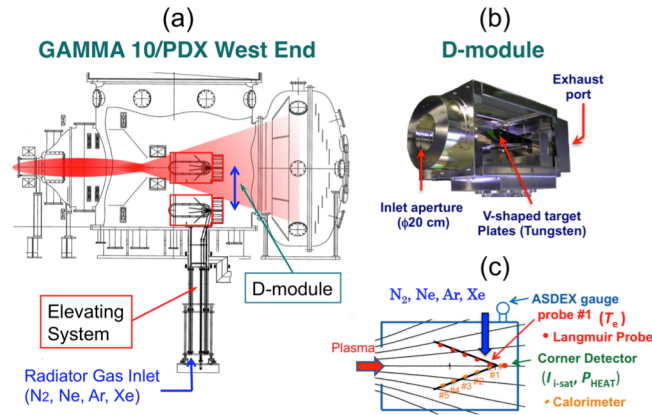


FIGURE 6. (a) Schematic view of the GAMMA 10/PDX west end-cell, (b) photograph of D-module, (c) D-module and experimental setup for detached plasma formation.

In order to compare the radiation cooling effects of various radiator gases, four kinds of gases (Xe, Ar, Ne and N₂) were examined in terms of the plasma parameters towards the plasma detachment in D-module. In Fig. 8, plasma parameters measured in D-module are plotted as a function of the pressure in D-module measured with ASDEX gauge. In this figure, the pressures of the following three gases (Ne, N₂ and Xe) are not absolutely calibrated. So that, these data are relatively corrected based on the sensitivity against the different gases of standard ionization gauge, since the sensitivity ratio between H₂ and Ar is almost the same as that obtained from the standard one. As shown in the figure, it is found that Xe has the strongest effects on electron cooling and reduction of heat and ion fluxes. T_e decreases down to 2 eV at the pressure of less than 1 Pa of Xe gas. The ion flux and the heat flux are also reduced to 4 % and 1%, respectively at 4 Pa. On the other hand, Ne is less effective in all the parameters. In the case of Ne, the reduction of T_e is small (down to 6 eV) and a relatively small amount of reduction in heat flux (30%) and ion flux (60%) are observed. From the above result, Neon has less effective on electron cooling and plasma detachment than Ar. In the case of N₂, T_e decreases to the same temperature as the case of Ar. Furthermore, the ion flux is more reduced than that of Ar in comparatively lower gas density region (< 2 Pa).

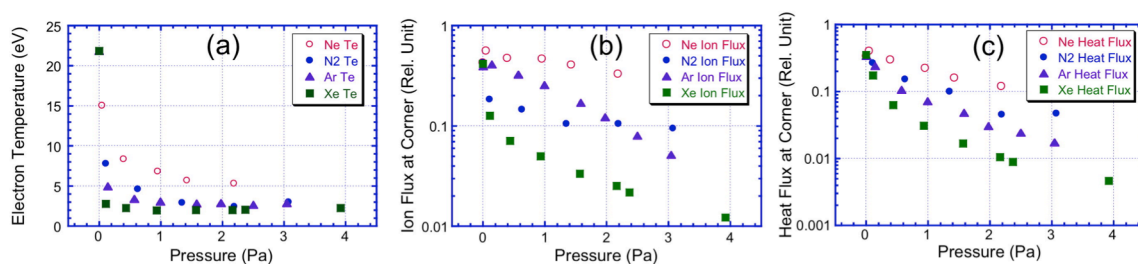


FIGURE 7. Dependence of (a) the electron temperature, (b) the ion flux and (c) the heat flux on the pressure in D-module.

2.3. Behavior of Recycling in GAMMA 10/PDX End-cell

It is a well-known fact that recycling phenomena is strongly affected by the wall temperature. However, the detailed mechanisms of recycling have not been clarified yet. The effect of wall temperature on the hydrogen recycling is also one of the most important issues for the particle balance study. In GAMMA 10/PDX, this effect has been investigated by using a temperature-controlled target installed in D-module and is exposed to the end

loss plasma. Figure 8 shows the schematic view of D-module, the base made of copper for fixing the tungsten plate in which the temperature control system is integrated and a typical example of temperature control experiments. The target temperature was heated in advance up to 573 K in order to minimize the effect of outgassing from the target. In the experiments of temperature change on the target plate, both $H\alpha$ intensity and electron density almost linearly increased with the target temperature and the $H\alpha$ intensity became twice due to the temperature increase from 384 K to 573 K. On the other hand, the electron density increases by 20%. The target temperature dependence was investigated under the hydrogen injection into D-module. It is found that according to increasing of hydrogen throughput, the enhancement of hydrogen recycling by high temperature target becomes small.

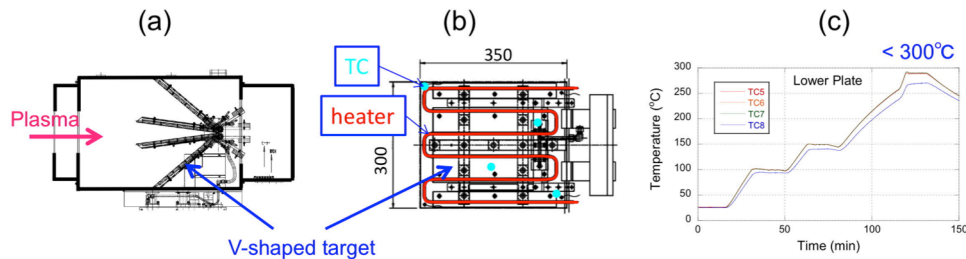


FIGURE 8. (a) Schematic view of D-module, (b) the target heating system, (c) temporal behavior of the target temperature.

3. DEVELOPMENT OF HIGH-POWER GYROTRON

3.1. Development of Dual Frequency 28GHz/35GHz Gyrotron

Development of 28/35GHz dual frequency gyrotrons has been strongly desired in collaboration research programs. The design targets for the 28/35 GHz dual-frequency gyrotron are listed in Table 1. In the frequency range of 28 GHz, 2MW-3sec. and 0.4 MW-CW is targeted and in the frequency range of 35 GHz, 1 MW-1sec is expected. The magnetic field profile required for the two different oscillation modes is formed with a super-conducting magnet (SCM).

TABLE 1. Design target of 2MW Dual Frequency Gyrotron

28 GHz 2 MW Dual-frequency Gyrotron		
Frequency	28 GHz	34.77 GHz
Output Power	2 MW	0.4 MW
Pulse Width	3 s	CW
Output Efficiency	50% (with CPD)	
Beam Voltage	80 kV	70 kV
Beam Current	70 A	20 A
MIG	triode	
Cavity mode	TE _{8,5}	TE _{10,6}
Output mode	Gaussian like	
Output Window	Sapphire Double Disk	
Collector	Depressed Collector	
	Sweeping coils	

External view and structural cross-section view are shown in Figs. 9(a) and (b), respectively. The results of design calculation showed that the target output power for the 28/35 GHz dual-frequency gyrotron was achieved

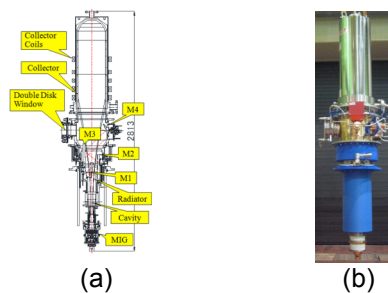


FIGURE 9. 2MW Dual-Frequency Gyrotron. (a) cross-section, (b) external view.

in these design values. Generated RF wave is converted to a Gaussian-like beam by a built-in quasi-optical mode converter. Then the RF wave is transmitted to the outside of the tube through an output window. The total transmission efficiency from the mode converter to the output window is calculated to be 97.4% at 28 GHz and 97.0% at 34.77 GHz, respectively.

3.2. Development of Dual Frequency Gyrotron Output Window

The dual-frequency gyrotron has a sapphire double-disk window so as to be used in CW operation. A structural cross-section view is shown in Fig. 10. Fluorocarbon coolant is flowed between the two sapphire disks. Before installing a double-disk window in the dual-frequency gyrotron, the dependence of its reflective power on coolant thickness was investigated through a cold test with 1 mW and a hot test using gyrotron output power of 600 kW. In the hot test, the reflective power was less than 2% at a coolant thickness of about 4 mm. The calculated absorbed power of the double-disk window was less than 1%.

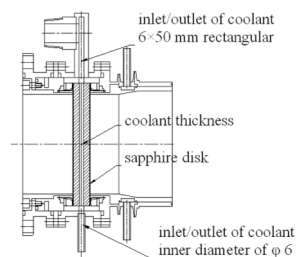


FIGURE 10. Sapphire double-disk window

3.3. Development of ECH system applied for divertor simulation studies

Development of ECH system and MW-power gyrotrons for the divertor simulation studies has been performed as a tool of generation and control of high heat-flux plasma flow [17]. Study on ELM simulation is also one of important subjects of urgent in divertor and PWI research and it has been requested that the development of intermittent heat source corresponds to the heat level of GW/m^2 .

The ELM simulation research has been carried out by using microwave source with gyrotrons and neutral beam source. In the case of ECH, repetitive pulse with 5 ms produces the intermittent plasma flow. Figure 11(a) shows the radial profile of the measured heat flux with a calorimeter installed at 30 cm downstream of the end-mirror exit. Improvement of the ECH antenna installed in the east plug/barrier-cell enhances the microwave intensity in the beam core and the increase of heat flux is recognized by 25 % in the center of the beam.

In Fig. 11(b), the energy density by one pulse of ECH Q_{heat} is plotted as a function of plug ECH power. The maximum value of the one pulse energy density is about 0.08 MJ/m^2 with 380 kW for 5 ms. According to the increasing ECH power, it is expected that the enhanced and controlled heat-flux enables the ELM-like heat load ($\geq 0.5 \text{ MJ/m}^2, 1 \text{ MW} \times 10\text{ms}$).

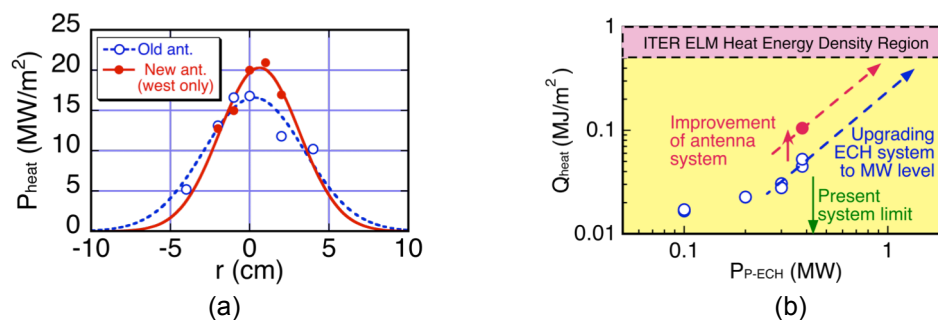


FIGURE 11. (a) Radial profile of the heat flux measured at 30 cm downstream. (b) Heat energy density as a function of the plug ECH power.

4. DIAGNOSTIC DEVELOPMENT

4.1. Thomson Scattering System in GAMMA 10/PDX

One of the most important development activities in diagnostics is multi-channel and multi-pass Thomson scattering system installed in the GAMMA 10/PDX central-cell. A neodymium-doped, yttrium–aluminum–garnet laser (Nd:YAG) Thomson scattering (TS) system was applied to measure electron temperature directly in the central-cell of GAMMA 10 in 2008. Figure 12 shows the schematic view of the TS system installed in the central. A horizontally polarized laser beam from YAG laser (Continuum, Powerlite 9010, 2 J/pulse, pulse width of 10 ns, 10 Hz, and beam diameter of about 9 mm) is used in this system and the beam is injected from the bottom port window of the central-cell. The scattered light is collected and reflected by a set of two Al:SiO₂-coated spherical mirrors with a curvature radius of 1.2 m and diameter of 0.6 m and 0.2 m, respectively. Finally at the light is focused to the nine channels of optical fiber bundle with a cross-section of $2 \times 7 \text{ mm}^2$ and the length of 6.67 m. Each channel optical fiber bundle is connected a 5-channel filter-type polychromator and the measuring range of electron temperature is designed to be from 10 eV to 1 keV. In this system, the scattering angle of 90° is adopted and the measurable radial positions are $X = 0, \pm 5, \pm 10, \pm 15,$ and $\pm 20 \text{ cm}$. Recently by adding a second collection mirror, polychromators and improvement of data acquisition system, measurement of radial six points in the 10 Hz repetition was achieved. In Fig. 13(a), an example of measured electron temperature is shown.

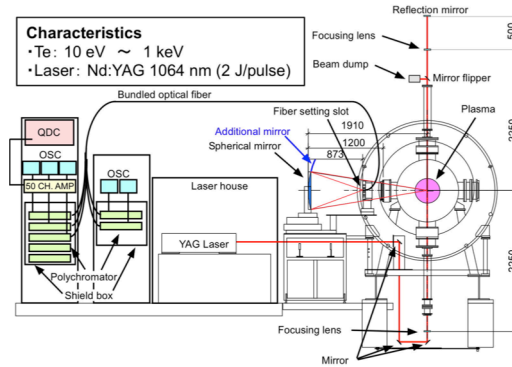


FIGURE 12. Schematic view of Thomson scattering system in the GAMMA 10/PDX central-cell.

In order to improve the TS signal intensity and time resolution, multi-pass (MP) TS systems were proposed [18]. The multi-pass Thomson scattering scheme effectively increases the scattering signal intensity from plasmas by the probing laser pulse to be focused multiple times onto the scattering volume [19, 20]. Construction of the polarization controlled multi-pass system was being built with the image relaying system in the system, which provided the highly time-resolved electron temperatures. Figure 13(b) shows the TS raw data and the pass numbers of TS signals are indicated in the case of multi-pass. As shown in the figure, about ten pass signals are identified and the signal intensity in the multi-pass is improved by about five times compared with the single pass case.

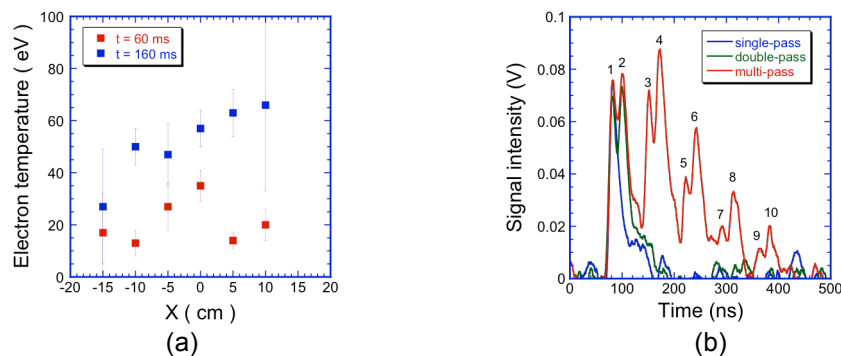


FIGURE 13. (a) Radial profile of the electron temperature. (b) Raw data of the scattered signal.

4.2. Microwave Interferometry in GAMMA 10/PDX End-Cell

A 60 GHz interferometer system using a local integrated antenna array (LIA) has been developed and installed in the E-divertor region. Figure 14(a) shows the schematic diagram of newly developed interferometer system. For this system, an eight-channel LIA has developed. Last year, installation of the system was completed and the density measurements in D-module have started [21]. Figure 14(b) shows the plenum pressure dependence of line-averaged density measured with the interferometer (open and closed circles) and the electron density measured by the nearest Langmuir probe (#4) on the target plate (cross), respectively. The electron density on the target plate increases up to around 600 mbar and then decreases in the higher plenum pressures. Measured line-averaged density is the order of 10^{17} - 10^{18} m^{-3} and shows a characteristic feature similar to those measured with the probe. By using this system, it is expected that more detailed information on the spatial structure of electron density will be clarified.

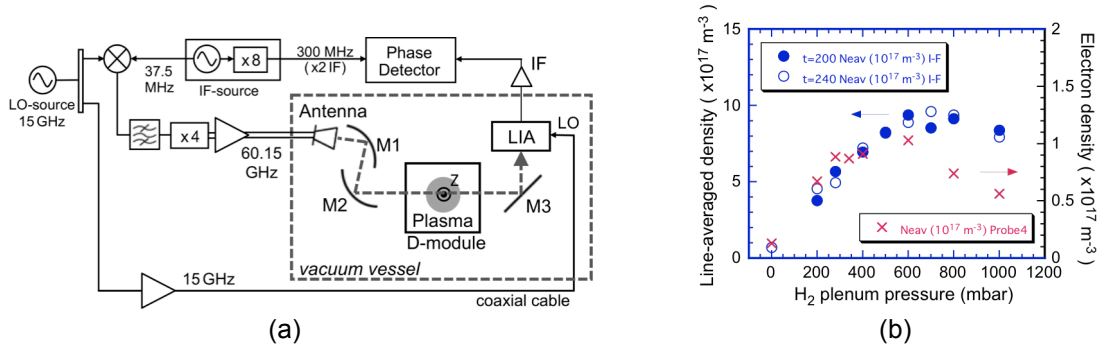


FIGURE 14. (a) Schematic diagram of the interferometer system using LIA. (b) Plenum pressure dependence of line-averaged density and those measured with probe (#4).

5. SUMMARY AND THE FUTURE

In recent years significant progress has been achieved in the GAMMA 10/PDX project on (1) divertor simulation studies, (2) development of gyrotrons and (3) diagnostics development as follows:

(1) Divertor simulation:

Additional ICRF heating at both anchor-cells together with the east plug/barrier ECH significantly increased the ion flux up to $3.3 \times 10^{23} / \text{m}^2 \text{ s}$ at the west end-mirror exit, which proved an effectiveness of additional plasma heating. Superimposing a short pulse of ECH onto the ICRF-heated plasma generates the maximum heat flux of $21 \text{ MW}/\text{m}^2$ by improving the west plug ECH antenna system, which exceeds the heat-load of ITER divertor plates. Comparison experiments of various radiator gases (Xe, Ar, Ne, N₂) injected into the divertor simulation experimental module (D-module) showed that Xe was the most effective gas on electron cooling and reduction of heat and ion fluxes. However, Ne is less effective. In low pressure region, N₂ has similar effects to Ar.

(2) Development of gyrotrons:

High-power gyrotrons in MW level have been successfully developed under collaboration with NIFS, Universities, QST and TETD. High performance plasma (high T_e and n_e) has been achieved in LHD by using total injection power of ECH > 5MW. High plasma current was non-inductively attained with 28 GHz injection in QUEST. Dual frequency, 1.38 MW at 28 GHz and 0.87 MW at 35 GHz was achieved. Fabrication of multi-MW dual-frequency 28/35 GHz first tube have been accomplished and oscillation test is in progress.

(3) Diagnostic development:

Multi-channel/multi-pass Thomson scattering system has been developed and simultaneous measurement of radially 6 points with 10 Hz can be available. Microwave interferometer system has been developed for divertor simulation plasma in D-module, which contributes to more detailed diagnostics in E-Divertor studies.

As future prospects, the following plans are considered: For divertor simulation studies, we will challenge the highest heat flux $>30 \text{ MW}/\text{m}^2$ by using new ECH antennae in both plug/barrier-cells. In the study using D-module, experiments of radiation cooling and characterization of plasma detachment under various radiator gas injection (Xe, Ar, Kr, Ne, N₂, etc.). For the further particle flux generation experiment using ICRF waves, we have a plan to enhance the particle flux optimizing the antenna structure and then will try to heating of end-loss plasma in the plug/barrier-cell toward the achievement of $10 \text{ MW}/\text{m}^2$ by only ICRF. For the development of high-power gyrotrons, multi-MW gyrotrons are in progress for realization of higher heat-flux / ELM simulation.

Another activity of gyrotron development is an international collaboration between Tsukuba and foreign institute such as Princeton Plasma Physics Laboratory (28/35 GHz 1.5-2 MW gyrotron tube).

In parallel with the above research activity, conceptual design work of new device has been started. This device consists of a relatively smaller (≤ 10 m) axisymmetric mirror system and its objective is to obtain highly-reliable extrapolative data-base as a pilot device towards the construction of the future actual divertor plasma generator (GAMMA/PDX-SC, tentatively) by making best use of the knowledge from GAMMA 10 /PDX.

ACKNOWLEDGMENTS

The authors thank the members of the GAMMA 10/PDX group of the University of Tsukuba and a number of collaboration researchers in many universities and institutes under the bi-directional collaboration research program. This work was partially supported by NIFS collaboration research programs. Main collaboration program numbers are as follows; NIFS14KUGM086, NIFS14KUGM090, NIFS13KUGM083, NIFS11KUGM050, NIFS15KUGM102, NIFS16KUGM117, NIFS-KOAH025.

REFERENCES

- [1] M. Inutake *et al.*, Phys. Rev. Lett. **55**, 939 (1985).
- [2] T. Imai *et al.*, Trans. Fusion Sci. Technol. **63** No.1T, 8 (2013).
- [3] Y. Nakashima *et al.*, Fusion Eng. Design volume **85** issue 6, 956 (2010).
- [4] Y. Nakashima *et al.*, Trans. Fusion Sci. Technol. **59** No.1T, 61 (2011).
- [5] K. Ichimura *et al.*, Plasma Fusion Res. **7**, 2405147 (2012).
- [6] Y. Nakashima *et al.*, J. Nucl. Mater. **438**, S738 (2013).
- [7] Y. Nakashima *et al.*, Trans. Fusion Sci. Technol. **63** No.1T, 100 (2013).
- [8] M. Sakamoto *et al.*, Trans. Fusion Sci. Technol. **63**, 188 (2013)
- [9] I. Uytendhouwen *et al.*, Plasma & Fusion Science **996** (2007) AIP proc. 17th RUSFD, pp. 159-165.
- [10] Y. Nakashima *et al.*, J. Nucl. Mater. **463**, 537 (2015).
- [11] Y. Nakashima *et al.*, Fusion Sci. Technol. **68**, 28 (2015).
- [12] T. Saito *et al.*, J. Plasma Fusion Res. **81**, 288 (2005).
- [13] A. Mase *et al.*, Nucl. Fusion **31**, 1725 (1991).
- [14] T. Kariya *et al.*, Fusion Sci. Tech. **55**, 91 (2009).
- [15] T.Kariya *et al.*, J. Infrared, Millim. Terahertz Waves **32**, 295 (2011).
- [16] G. Haas *et al.*, J. Nucl. Mater. **121**, 151 (1984).
- [17] R. Minami *et al.*, Fusion Sci. Technol. **68**, 142 (2015).
- [18] M. Yoshikawa *et al.*, Rev. Sci. Instrum. **83**, 10E333 (2012).
- [19] M. Yoshikawa *et al.*, Plasma and Fusion Res. **8**, 1205169 (2013).
- [20] M. Yoshikawa *et al.*, Rev. Sci. Instrum. **85**, 11D801 (2014).
- [21] J. Kohagura *et al.*, J. Instrum. **10**, C12024 (2015).